Outage Analysis of AmBC-Enabled Vehicular Communications under Mixed Nakagami-m and Cascaded Nakagami-m Fading Channels

Ashutosh Rastogi[1], Suneel Yadav[1], Radhika Gour[1], and Devendra Singh Gurjar[2]

Abstract— Ambient backscatter communication (AmBC) is proposed as a prominent technology to support energy-efficient low power transmissions in 6G and beyond wireless networks. AmBC is capable of providing battery-free connectivity among large scale Internet-of-Things (IoT) devices. Also, it can satisfy the stringent delay and power saving requirements of intelligent transport systems (ITS) in seeking diverse vehicular applications. Motivated by these emerging trends, we consider an AmBC-assisted tag-reader-based vehicular scenario and carried out the outage analysis by deriving the exact expressions for the reader's outage probability (OP) considering tag being in reflective or non-reflective state over mixed Nakagami-m and double Nakagami-m fading environment. We also examine the asymptotic OP in the high signal-to-noise (SNR) regime, which is perfectly aligned with the exact OP values even at moderate SNRs. Further, this asymptotic analysis reveals some meaningful insights into the systems diversity order. Numerical and simulation studies are conducted to validate our mathematical framework.

I. INTRODUCTION

Wireless communication systems have witnessed phenomenal growth over the past two decades, and upcoming 6G and beyond networks are expected to fulfill the requirements of a fully connected digital world which provides ubiquitous wireless connectivity for diversified applications [1]. The advancement in Internet-of-Things (IoT) systems may further support the seamless wireless connectivity of enormous number of intelligent devices (e.g., wearable devices, renewable sensors, tags) [2]. Therefore, a massive data collection, storage, and information exchange among the various IoT devices have posed several serious challenges in terms of throughput, delay, and power consumption. Moreover, by looking into the incremental growth in the number of on-road vehicles, Intelligent Transportation System (ITS) is seeking for the potential solutions to enable more reliable communication among moving vehicles forming Internet-of-Vehicles (IoV) infrastructure. IoV, as an integral part of ITS, provides a habitat for self-organizing vehicles to enable advanced vehicular applications, such as, active safety, traffic efficiency, and environmental protection [3]. In practice, vehicles are equipped with advanced battery-driven sensors to collect and exchange the information in the IoV networks. These devices restrain the usage of IoT-enabled ITS applications due to power and range constraints. Thus, the power requirement of such battery driven devices can interrupt the connectivity and hence reliable vehicular communication can be lost.

Recently, ambient backscatter communication (AmBC) has been considered a promising solution to combat these challenges as it can provide battery-free transmissions among various IoT devices by harvesting the energy from available radio frequency (RF) signals in the surroundings, such as, digital television (TV) broadcasting, FM, cellular or Wireless-Fidelity (Wi-Fi) signals [4]. AmBC can make sensors and passive tags battery-free, reducing human intervention in recharging or replacing the batteries. A typical AmBC system mainly comprises of three components; an ambient source, a reader, and a tag. In general, the complete information exchange process occurs in three steps [5]; i) the tag harvests energy from surroundings and stores it; ii) the tag separately modulate bit '1' or bit '0' that indicates the backscattering of signal or absorption of the signal, respectively; and iii) reader performs the decoding and demodulates the corresponding bit from the received backscattered signal. The AmBC-enabled communication has recently attracted more research attention in the literature [6]-[18] and the references therein.

Specifically, in [6], the authors investigated an AmBC system by designing a front-end and high-gain antenna for tag and reader in order to extend the transmission range of the system. Such systems can be well suited for vehicle-to-infrastructure (V2I) scenario. The performance of a wireless powered device-to-device (D2D) communication system is analyzed in [7] with integrated ambient backscatter devices. Several demodulation schemes and bit error rate (BER) performance of AmBC systems are discussed in [8]-[10]. The ergodic capacity and outage probability (OP) expressions are derived for the backscatter links by considering real or complex RF signals in [11]. In [12], the authors have done the outage analysis of a backscatter transmission with maximum ratio combining processing at the reader with an adaptive mechanism that opportunistically utilizes the part or full battery power to ensure that the backscatter signal is not restrained abruptly. In [13], the authors discussed a resource allocation framework for the AmBC-equipped non-orthogonal multiple access enabled IoV networks, where imperfect successive interference cancellation decoding is considered. Moreover, IoV networks include both vehicle-to-vehicle (V2V) and vehicle-to-fixed infrastructure (V2I) links. Due to mobility of vehicles, the traditional Rayleigh/Nakagami-m fading channel does not characterize the V2V links precisely, as vehicular nodes are not stationary. Though from the field measurement and theoretical analysis point of view, cascaded (such as, double-Rayleigh/double Nakagami-m) channel modeling is shown to be more appropriate in characterizing the non-stationary V2V links as described in [14]-[17]. Most of the works that have been discussed above mainly deal with the

[1]A. Rastogi, S. Yadav, and R. Gour are with the Department of ECE, Indian Institute of Information Technology Allahabad, Prayagraj, 211015, India {`rse2020502, suneel, and radhika`}`@iiita.ac.in`
[2]D. S. Gurjar is with the Department of ECE, National Institute of Technology Silchar, Assam, India `devendra.gurjar@ieee.org`
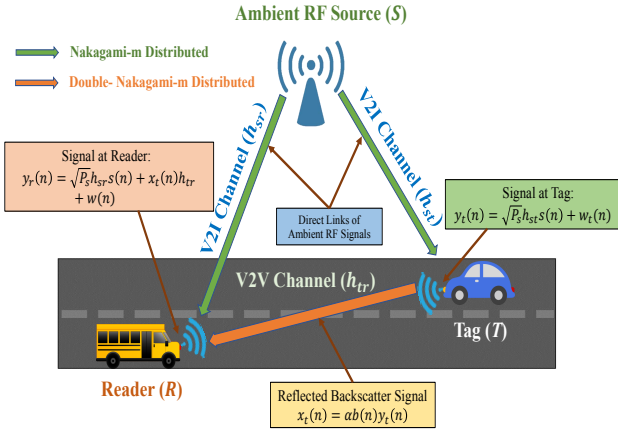
Fig. 1: An illustration of ambient backscatter empowered vehicular communication system.

static scenario, whereas the authors in [18] utilized selection combining diversity scheme to perform the outage analysis of AmBC system while considering a moving reader and multiple stationary tags. However, to the best of authors' knowledge, the OP analysis of AmBC-assisted vehicular communication systems under mixed Nakagami-m fading (for V2I links) and double Nakagami-m fading (for V2V links) has not been analyzed in the literature.

Motivated by the above discussion, in this paper, we study the performance of AmBC-enabled vehicular communication systems by characterizing the V2I channel and V2V channel as Nakagami-m fading and double Nakagami-m fading, respectively. Particularly, we derive the exact expression for the OP of the considered system, and perform the asymptotic OP analysis in the high signal-to-noise ratio (SNR) regime to get the insights about the system's diversity order. Further, we present the numerical and simulation results to verify our analytical framework.

Notations: $F_X(\cdot)$ and $f_X(\cdot)$ are the cumulative distribution function (CDF) and probability density function (PDF) of X. $G_{p,q}^{m,n}\left(x\big|_{b_1,\ldots,b_q}^{a_1,\ldots,a_p}\right)$ is the Meijer-G function [19, eq. (9.301)], and $\Gamma(\cdot)$ is the complete Gamma function and $\Upsilon(\cdot,\cdot)$ is the lower incomplete Gamma function [19, eq. (8.350)].

II. SYSTEM AND CHANNEL MODELS

We consider an ambient backscatter-enabled vehicular communication network, as shown in Fig. 1, which consists of a reader (R), a wireless-powered battery-less tag (T), and an ambient RF source (S). Here, S is assumed to be a fixed infrastructure, whereas T and R are mounted over the vehicles, such as, bus, car, etc. Particularly, the information transfer from S to R (i.e., $S \rightarrow R$) and S to T (i.e., $S \rightarrow T$) enables V2I type of communication, while a V2V type of communication is carried out when information is transferred from T to R, (i.e., $T \rightarrow R$). We further assume that all the nodes have single-antenna and operate in a half-duplex mode. The channels associated with the links $S \rightarrow T$, $S \rightarrow R$, and $T \rightarrow R$ are denoted as h_{st}, h_{sr}, and h_{tr}, respectively, and assumed to be reciprocal, quasi-static

and, experience independent and non identically distributed (i.ni.d.) fading. Specifically, we consider that the channel coefficients h_{st}, h_{sr}, and h_{tr}, are Nakagami-m, Nakagami-m, and double Nakagami-m distributed, respectively. The V2I channel coefficient h_ϕ is modeled as $\text{Nak}(m_\phi, \Omega_\phi)$, for $\phi \in \{st, sr\}$. Moreover, the V2V channel coefficient h_{tr} is modeled as the product of two i.ni.d Nakagami-m random variables, i.e., $h_{tr,1}$ and $h_{tr,2}$, such that $h_{tr} = h_{tr,1}h_{tr,2}$, where $h_{tr,j} \sim \text{Nak}(m_{tr,j}, \Omega_{tr,j})$ with $j \in \{1,2\}$. The noise at the nodes is modeled as additive white Gaussian noise (AWGN) with zero mean and variance N_0.

A. Instantaneous end-to-end SNR

In the considered network, the received ambient RF signal at T can be expressed as

$$y_t(n) = \sqrt{P_s}h_{st}s(n) + w_t(n), \qquad (1)$$

where $s(n)$ denotes the unit energy signal, P_s is the average transmit power, and $w_t(n)$ is the noise incurred within T.

Now, T uses the received signal $y_t(n)$ for sending its own binary data $b(n) \in \{0,1\}$ via backscattering the RF source signal $s(n)$ or not. If $b(n) = 0$, then T operates in non-reflecting state, whereas if $b(n) = 1$, the signal from T can be backscattered towards the reader. Meanwhile, we can express the signal backscattered by T as $x_t(n) = \alpha b(n)y_t(n)$, where $\alpha \in [0,1]$ is the reflection coefficient of the antenna inside T. Thus, the signal received at R, $y_r(n)$, can be given as

$$y_r(n) = \underbrace{\sqrt{P_s}h_{sr}s(n)}_{\text{direct RF signal}} + \underbrace{h_{tr}x_t(n)}_{\text{backscattered signal}} + \underbrace{w(n)}_{\text{noise}}$$

$$= \sqrt{P_s}h_{sr}s(n) + \alpha b(n)h_{tr}(\sqrt{P_s}h_{st}s(n) + w_t(n)) + w(n)$$

$$\overset{(a)}{=} \sqrt{P_s}h_{sr}s(n) + \sqrt{P_s}\alpha b(n)h_{st}h_{tr}s(n) + w(n), \qquad (2)$$

where (a) is obtained by neglecting the thermal noise $w_t(n)$, i.e., $w_t(n) \approx 0$. This assumption is reasonable as T is a passive element and does not possess large signal processing operations [20]. $w(n)$ denotes the AWGN noise at R.

We can further represent (2) under the non-reflecting state, i.e., $b(n) = 0$, and reflecting state, i.e., $b(n) = 1$, as

$$y_r(n) = \begin{cases} \sqrt{P_s}h_0 s(n) + w(n); & b(n) = 0, \\ \sqrt{P_s}h_1 s(n) + w(n); & b(n) = 1, \end{cases} \qquad (3)$$

where $h_0 \triangleq h_{sr}$ and $h_1 \triangleq h_{sr} + \alpha h_{st}h_{tr}$.

Using (3), the instantaneous end-to-end SNR at R for two states '0' and '1' can be expressed as

$$\wedge_i = \frac{P_s|h_i|^2}{N_0}, \qquad (4)$$

for $i \in \{0, 1\}$.

B. The V2I and V2V fading channel distributions

The channel coefficients corresponding to V2I channels, i.e., h_{sr} and h_{st}, undergo Nakagami-m fading distribution, therefore, the CDFs and PDFs of $|h_\phi|^2$, for $\phi \in \{st, sr\}$, can be expressed, respectively, as $F_{|h_\phi|^2}(x) = \frac{1}{\Gamma(m_\phi)}\Upsilon(m_\phi, \frac{m_\phi}{\Omega_\phi}x), x > 0$ and $f_{|h_\phi|^2}(x) = \frac{1}{\Gamma(m_\phi)}\left(\frac{m_\phi}{\Omega_\phi}\right)^{m_\phi}x^{m_\phi-1}e^{-\frac{m_\phi}{\Omega_\phi}x}, x > 0$. Moreover, the channel coefficient pertaining to V2V link undergoes double

Nakagami-m fading distribution, and hence the CDF and PDF of the channel gain $|h_{tr}|^2$ can be given as [21]-[23]

$$F_{|h_{tr}|^2}(x) = \frac{1}{\Gamma(m_{tr_1})\Gamma(m_{tr_2})} G_{1,3}^{2,1}\left[x\zeta_{tr}\Big|_{m_{tr_1},m_{tr_2},0}^{1}\right], x > 0, \tag{5}$$

$$f_{|h_{tr}|^2}(x) = \frac{1}{x\Gamma(m_{tr_1})\Gamma(m_{tr_2})} G_{0,2}^{2,0}\left[x\zeta_{tr}\Big|_{m_{tr_1},m_{tr_2}}^{-}\right], x > 0, \tag{6}$$

respectively, where $\zeta_{tr} = \frac{m_{tr_1} m_{tr_2}}{\Omega_{tr_1}\Omega_{tr_2}}$.

III. PERFORMANCE ANALYSIS

In this section, we evaluate the OP and asymptotic OP expressions for the considered AmBC network under mixed Nakagami-m and double Nakagami-m fading channels. To proceed further, we first need to evaluate the CDF and PDF of $h_1 \triangleq h_{sr} + \alpha h_{st} h_{tr}$. To do so, we require the statistics of $\xi \triangleq \alpha h_{st} h_{tr}$, which is a triple Nakagami-m distributed. In the sequel, we derive the distributions of ξ and h_1.

A. The CDFs and PDFs of $\xi \triangleq \alpha h_{st} h_{tr}$ and $h_1 \triangleq h_{sr} + \xi$.

1) The CDF and PDF of $\xi \triangleq \alpha h_{st} h_{tr}$: The CDF and PDF of ξ are given in the following proposition.

Proposition 1: The CDF and PDF of the channel gain ξ under mixed Nakagami-m and double Nakagami-m fading can be expressed, respectively, as

$$F_\xi(x) = \frac{1}{\Gamma(m_{st})\Gamma(m_{tr_1})\Gamma(m_{tr_2})} G_{1,4}^{3,1}\left[x^2\lambda_{tr}\Big|_{m_{st},m_{tr_1},m_{tr_2},0}^{1}\right], \tag{7}$$

$$f_\xi(x) = \frac{2}{x\Gamma(m_{st})\Gamma(m_{tr_1})\Gamma(m_{tr_2})} G_{0,3}^{3,0}\left[x^2\lambda_{tr}\Big|_{m_{st},m_{tr_1},m_{tr_2}}^{-}\right], \tag{8}$$

where $\lambda_{tr} = \frac{m_{st}\zeta_{tr}}{\alpha^2\Omega_{st}}$.

Proof: See Appendix A for the derivation. ∎

2) The CDF and PDF of h_1: The CDF and PDF of $h_1 \triangleq h_{sr} + \alpha h_{st} h_{tr}$ under mixed Nakagami-m and double Nakagami-m fading can be derived as per Proposition 2.

Proposition 2: The CDF and PDF of h_1 can be given as

$$F_{h_1}(x) = \sum_{n=0}^{\infty} \frac{(-1)^n}{n!(m_{sr}+n)} \frac{\Gamma(2m_{sr}+2n+1)\left(\frac{m_{sr}}{4\Omega_{sr}}\right)^{m_{sr}+n}}{\Gamma(m_{st})\Gamma(m_{tr_1})\Gamma(m_{tr_2})\Gamma(m_{sr})}$$
$$\times x^{2(m_{sr}+n)} G_{2,5}^{3,2}\left(\frac{\Theta x^2}{\alpha^2}\Big|_{m_{st},m_{tr_1},m_{tr_2},-(m_{sr}+n),\epsilon}^{\frac{1}{2},1}\right), \tag{9}$$

$$f_{h_1}(x) = \sum_{n=0}^{\infty} \frac{2(-1)^n}{n!(m_{sr}+n)} \frac{\Gamma(2m_{sr}+2n+1)}{\Gamma(m_{st})\Gamma(m_{tr_1})\Gamma(m_{tr_2})\Gamma(m_{sr})}$$
$$\times x^{2(m_{sr}+n)-1}\left(\frac{m_{sr}}{4\Omega_{sr}\alpha^2}\right)^{m_{sr}+n}$$
$$\times G_{3,6}^{3,3}\left(\frac{\Theta x^2}{\alpha^2}\Big|_{m_{st},m_{tr_1},m_{tr_2},-(m_{sr}+n),\epsilon,(1-m_{sr}-n)}^{-(m_{sr}+n),\frac{1}{2},1}\right), \tag{10}$$

where $\Theta = \frac{m_{st}m_{tr_1}m_{tr_2}}{\Omega_{st}\Omega_{tr_1}\Omega_{tr_2}}$ and $\epsilon = \frac{1-2m_{sr}-2n}{2}$.

Proof: The detailed proof is given in Appendix B. ∎

B. OP Analysis

An outage occurs when the received instantaneous SNR at R becomes lower than a certain preset threshold η_{th} [24]. Therefore, the OP under two states, i.e., $b(n) = 0$ and $b(n) = 1$, can be expressed as

$$\mathcal{P}_{\text{out}}(\eta_{th}) = p_0 \underbrace{\Pr\left[\wedge_0 \le \eta_{th}\right]}_{\triangleq \mathcal{P}_{\text{out}|0}(\eta_{th})} + p_1 \underbrace{\Pr\left[\wedge_1 \le \eta_{th}\right]}_{\triangleq \mathcal{P}_{\text{out}|1}(\eta_{th})}, \tag{11}$$

where p_0 and p_1 are *apriori* probabilities pertaining to $b(n) = 0$ and $b(n) = 1$, respectively.

By utilizing the definition of $\wedge_i$, for $i \in \{0, 1\}$, from (4), we can express $\mathcal{P}_{\text{out}|i}(\eta_{th})$ as

$$\mathcal{P}_{\text{out}|i}(\eta_{th}) = \Pr\left[\rho|h_i|^2 \le \eta_{th}\right]$$
$$= F_{|h_i|^2}\left(\frac{\eta_{th}}{\rho}\right), \tag{12}$$

where $\rho = \frac{P_s}{N_0}$ denotes the average transmit SNR.

1) Calculation of $\mathcal{P}_{out|0}(\eta_{th})$: Under Nakagami-$m$ fading channel, the CDF of the channel gain $|h_0|^2 \triangleq |h_{sr}|^2$ for the state $b(n) = 0$ is given by $F_{|h_0|^2}(x) = \frac{1}{\Gamma(m_{sr})}\Upsilon\left(m_{sr}, \frac{m_{sr}}{\Omega_{sr}}x\right)$, and hence $\mathcal{P}_{\text{out}|0}(\eta_{th})$ in (12) can be represented as

$$\mathcal{P}_{\text{out}|0}(\eta_{th}) = \frac{1}{\Gamma(m_{sr})}\Upsilon\left(m_{sr}, \frac{m_{sr}}{\Omega_{sr}}\frac{\eta_{th}}{\rho}\right). \tag{13}$$

2) Calculation of $\mathcal{P}_{out|1}(\eta_{th})$: The CDF of $|h_1|^2$ for the state $b(n) = 1$ can be obtained by replacing x^2 with x in (9), and subsequently utilizing it in (12), we can get $\mathcal{P}_{\text{out}|1}(\eta_{th})$ as

$$\mathcal{P}_{\text{out}|1}(\eta_{th}) = \sum_{n=0}^{\infty} \frac{(-1)^n}{n!(m_{sr}+n)} \frac{1}{\Gamma(m_{st})\Gamma(m_{tr_1})\Gamma(m_{tr_2})}$$
$$\times \frac{\Gamma(2m_{sr}+2n+1)}{\Gamma(m_{sr})}\left(\frac{m_{sr}\eta_{th}}{4\Omega_{sr}\rho}\right)^{m_{sr}+n}$$
$$\times G_{2,5}^{3,2}\left(\frac{\Theta}{\alpha^2}\frac{\eta_{th}}{\rho}\Big|_{m_{st},m_{tr_1},m_{tr_2},-(m_{sr}+n),\epsilon}^{\frac{1}{2},1}\right). \tag{14}$$

Finally, the overall OP can be obtained by invoking $\mathcal{P}_{\text{out}|0}(\eta_{th})$ and $\mathcal{P}_{\text{out}|1}(\eta_{th})$ from (13) and (14), respectively, into (11).

Remark 1: We can see from the OP expression that it consists Meijer-G function and some elementary functions, whose evaluation can be carried out using Mathematica software for various involved system parameters. In addition, the OP expression includes infinite summation term, which converges quickly as can be verified using ratio test,[1] hence making our analysis well suited for practical use cases.

C. Asymptotic OP Analysis

Here, we derive the asymptotic OP expression in the high SNR regime, i.e. $\rho \to \infty$, to reveal more insights about the considered AmBC-enabled vehicular communication system under mixed Nakagami-m and double Nakagami-m fading

---

[1]For any infinite series $\sum_0^\infty f_\tau$, let $S := \lim_{\tau \to \infty}\left|\frac{f_{\tau+1}}{f_\tau}\right|$. According to [25], the series is convergent if $S < 1$, divergent if $S > 1$, and inconclusive if $S = 1$.

channels. The overall asymptotic OP expression of the considered system can be given as

$$\mathcal{P}_{\text{out}}^{\text{asy}}(\eta_{th}) = p_0 \mathcal{P}_{\text{out}|0}^{\text{asy}}(\eta_{th}) + p_1 \mathcal{P}_{\text{out}|1}^{\text{asy}}(\eta_{th}), \qquad (15)$$

where $\mathcal{P}_{\text{out}|0}^{\text{asy}}(\eta_{th})$ and $\mathcal{P}_{\text{out}|1}^{\text{asy}}(\eta_{th})$ are the asymptotic OP for the transmission states $b(n) = 0$ and $b(n) = 1$, respectively.

1) Calculation of $\mathcal{P}_{out|0}^{asy}(\eta_{th})$: By applying the approximation $\Upsilon(\alpha, z) \underset{z \to 0}{\approx} \frac{z^\alpha}{\alpha}$ under the high SNR regime ($\rho \to \infty$) in (13), the asymptotic OP expression for the state $b(n) = 0$ can be expressed as

$$\mathcal{P}_{\text{out}|0}^{\text{asy}}(\eta_{th}) \simeq \frac{1}{\Gamma(m_{sr}+1)} \left(\frac{m_{sr}\eta_{th}}{\Omega_{sr}} \right)^{m_{sr}} \left(\frac{1}{\rho} \right)^{m_{sr}}. \quad (16)$$

2) Calculation of $\mathcal{P}_{out|1}^{asy}(\eta_{th})$: From (14), it is seen that as n increases the $\mathcal{P}_{\text{out}|1}(\eta_{th})$ decreases quickly with the increase in SNR, as it is proportional to $\frac{1}{\rho^n}$. Therefore, by retaining the first term, i.e., $n = 0$, and ignoring other infinitesimal terms in (13) under high SNR regime, the asymptotic OP expression $\mathcal{P}_{\text{out}|1}^{\text{asy}}(\eta_{th})$ for the state $b(n) = 1$ can be expressed as

$$\mathcal{P}_{\text{out}|1}^{\text{asy}}(\eta_{th}) = \left(\frac{\eta_{th}m_{sr}}{4\Omega_{sr}} \right)^{m_{sr}} \frac{\Gamma(2m_{sr}+1)}{\Gamma(m_{st})\Gamma(m_{tr_1})\Gamma(m_{tr_2})(m_{sr})!}$$
$$\times \left(\frac{1}{\rho} \right)^{m_{sr}} G_{2,5}^{3,2} \left(\frac{\Theta\eta_{th}}{\rho\alpha^2} \Big|_{m_{st}, m_{tr_1}, m_{tr_2}, -m_{sr}, \frac{1-2m_{sr}}{2}}^{\frac{1}{2}, 1} \right). \quad (17)$$

Furthermore, the overall asymptotic OP can be obtained by invoking the expressions of $\mathcal{P}_{\text{out}|0}^{\text{asy}}(\eta_{th})$ and $\mathcal{P}_{\text{out}|1}^{\text{asy}}(\eta_{th})$ from (16) and (17), respectively, into (15) as

$$\mathcal{P}_{\text{out}}^{\text{asy}}(\eta_{th}) = \left[p_0 \frac{\left(\frac{m_{sr}\eta_{th}}{\Omega_{sr}} \right)^{m_{sr}}}{\Gamma(m_{sr}+1)} + p_1 \left(\frac{\eta_{th}m_{sr}}{4\Omega_{sr}} \right)^{m_{sr}} \right.$$
$$\times \frac{\Gamma(2m_{sr}+1)}{\Gamma(m_{st})\Gamma(m_{tr_1})\Gamma(m_{tr_2})(m_{sr})!}$$
$$\left. \times G_{2,5}^{3,2} \left(\frac{\Theta\eta_{th}}{\rho\alpha^2} \Big|_{m_{st}, m_{tr_1}, m_{tr_2}, -m_{sr}, \frac{2m_{sr}-1}{2}}^{\frac{1}{2}, 1} \right) \right] \left(\frac{1}{\rho} \right)^{m_{sr}}. \tag{18}$$

Remark 2 (Diversity Order Analysis): Substituting (18) into the definition of the diversity order [22], i.e., $\mathbb{G}_{\mathbb{D}iv} = -\lim\limits_{\rho \to \infty} \frac{\mathcal{P}_{\text{out}}^{\text{asy}}(\eta_{th})}{\log(\rho)}$, and simplifying for $\rho \to \infty$, we can infer that the diversity order of m_{sr} can be achieved.

IV. NUMERICAL AND SIMULATION RESULTS

This section verifies the effectiveness of our proposed analytical findings through the numerical and simulation results using Mathematica and Matlab software, respectively. The Monte-Carlo simulations are averaged over 10^5 independent trials. For numerical investigations, we assume $p_0 = p_1 = \frac{1}{2}$, i.e., the occurrence of both the states is equiprobable. Moreover, we assume $m_{tr_1} = m_{tr_2} = m_{tr}$ for simplicity in the numerical analysis with various system parameters.

Fig. 2 shows the OP performance for different values of threshold (η_{th}) against average transmit SNR (ρ), where $\Omega_{st} = \Omega_{tr} = \Omega_{sr} = 1, m_{st} = m_{tr} = m_{sr} = 1$, and $\alpha = 0.5$. Here, we plot the exact OP and asymptotic OP curves according to (11) and (15). It is noted from this figure that the exact OP curves are perfectly aligned with the simulation results over the entire range of SNR. Also, the asymptotic
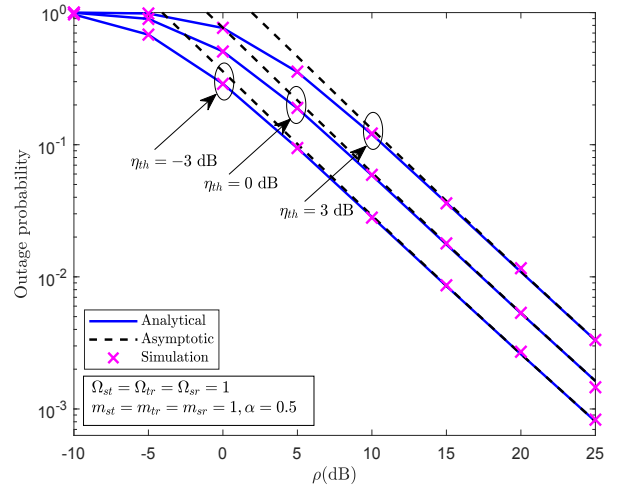

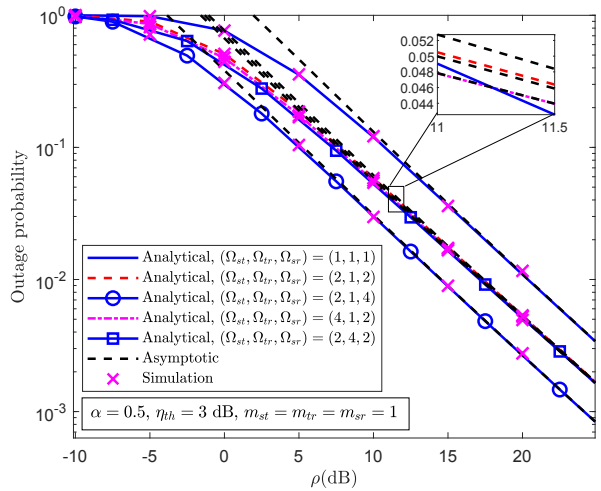Fig. 2: OP performance as a function of average transmit SNR (ρ).

Fig. 3: Impact of average channel variances on the OP performance.

curves coincide with the exact results in the medium-to-high SNR regime. As expected, a significant gain in OP performance is observed with the increased SNR, regardless of η_{th}. However, it is observed that the OP performance is degraded with increased value of η_{th}. The obvious reason behind this reduction is that more transmit power is required to attain higher target SNR threshold. In addition, it is worth verifying the diversity order of the considered system by looking into the asymptotic OP curves. For any given two points (x_1, y_1) and (x_2, y_2) on the asymptotic curves in Fig. 2, we can compute the slope of the curves by using $\frac{\log(y_1)-\log(y_2)}{\log(10^{\frac{x_1}{10}})-\log(10^{\frac{x_2}{10}})} = -m_{sr}$, which coincides with the diversity order analysis presented in Section III-C.

In Fig. 3, we present the impact of average channel variances (i.e., Ω_{st}, Ω_{tr}, and Ω_{sr}) on the OP performance of considered AmBC-assisted vehicular network. We set $\alpha = 0.5, m_{st} = m_{tr} = m_{sr} = 1$, and $\eta_{th} = 3$ dB. From the plotted curves, it is seen that the analytical results are in well agreement with simulation results. From this figure, we can
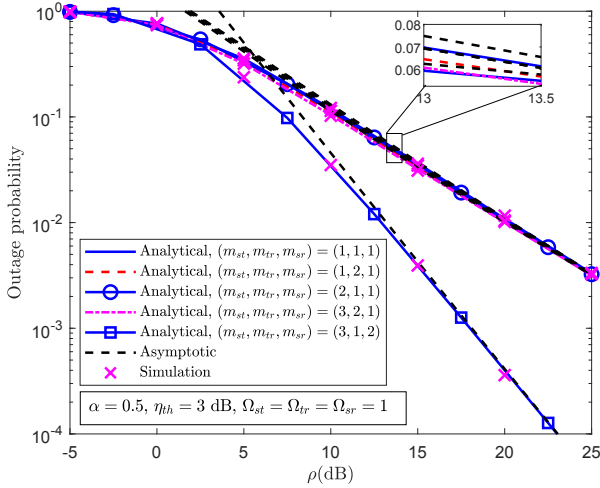
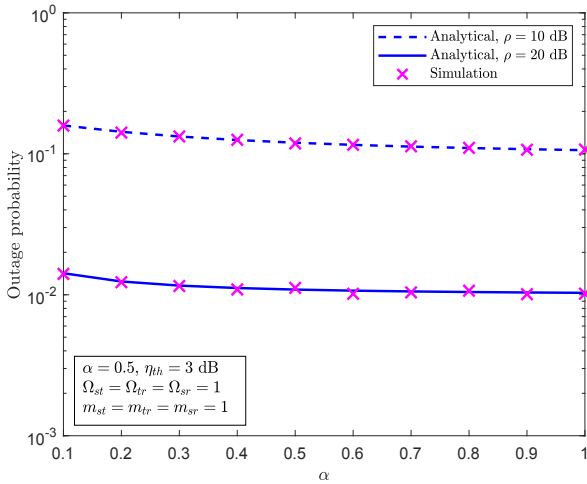Fig. 4: Impact of fading severity parameter on the OP performance.

Fig. 5: Impact of α on the OP performance.

easily see that the OP performance improves as the average channel gain increases. However, it is well emphasized that the OP performance gain is more significant when Ω_{sr} is higher than Ω_{st} and Ω_{tr}. This is due to the reason that the direct transmission from S to R contributes more to OP performance improvement compared to backscatter transmission, as the link $S \rightarrow R$ will always be available even when $S \rightarrow T \rightarrow R$ link is not available (i.e., the tag is not transmitting any signals rather the energy of the signal is completely absorbed).

In Fig. 4, we exemplify the impact of fading severity parameter (i.e., m_{st}, m_{tr}, and m_{sr}) on the OP performance for fixed $\alpha = 0.5, \Omega_{st} = \Omega_{tr} = \Omega_{sr} = 1$, and $\eta_{th} = 3$ dB. From the plotted curves, it is evident that the analytical and asymptotic results of OP are aligned with the simulation results. It is also worthy to mention that the OP performance improves as the values m_{st}, m_{tr}, and m_{sr} increase. More precisely, the value of m_{sr} is more dominant compared to other fading severity parameters, which is also evident by observing a drastic improvement in the OP performance.

Fig. 5 depicts the effect of attenuation factor α on the OP performance for the different transmit SNR $\rho = \{10, 20\}$ dB. For obtaining various results, we set $\Omega_{st} = \Omega_{tr} = \Omega_{sr} = 1, m_{st} = m_{tr} = m_{sr} = 1$, and $\eta_{th} = 3$ dB. We observe that for the given SNR value, the OP slightly decreases on increasing the attenuation factor, which is evident from the results and well complimented by the analytical expressions given in (14), as α is available in the denominator of the Meijer-G function. Hence, we can deduce that a high value of α is desirable for lower OP. Further, for obvious reasons, the OP performance improves considerably as ρ increases, irrespective of α values.

V. CONCLUSION

This paper investigated the outage performance of AmBC-empowered vehicular communication systems in a mixed Nakagami-m and cascaded Nakagami-m fading environment. We derived the effective channel distributions and analyzed the exact OP under the considered fading scenario. We then deduced the asymptotic OP expression in the high SNR regime and verified that the asymptotic OP is in well alignment with the exact values. We further analytically evaluated the system's diversity order of m_{sr} using the asymptotic expression. Finally, we validated our theoretical findings with the help of numerical and simulation results.

APPENDIX

A. Proof of Proposition 1

By defining $|\xi|^2 \triangleq |\alpha h_{st} h_{tr}|^2$, we can express the CDF of $|\xi|^2$ as

$$F_{|\xi|^2}(x) = \int_0^\infty F_{|h_{tr}|^2}\left(\frac{x}{\alpha^2 v}\right) f_{|h_{st}|^2}(v) dv. \quad (19)$$

Invoking the CDF of $|h_{tr}|^2$ from (5) and PDF of $|h_{st}|^2$ into (19), and further simplifying the integration using [26, eq. (07.34.21.0088.01)], we can obtain the result as

$$F_{|\xi|^2}(x) = \frac{1}{\Gamma(m_{st})\Gamma(m_{tr_1})\Gamma(m_{tr_2})}$$
$$\times G_{4,1}^{1,3}\left[\frac{1}{x\lambda_{tr}}\Big|_0^{1-m_{st},1-m_{tr_1},1-m_{tr_2},1}\right], \quad (20)$$

which can be then expressed as (7) via the identity [26, eq. (07.34.16.0002.01)] and the relation $F_\xi(x) = F_{|\xi|^2}(x^2)$.

Furthermore, differentiating (19) with respect to x and using the identity [26, eq. (07.34.16.0002.01)], we can obtain the PDF of ξ, as presented in (8).

B. Proof of Proposition 2

The CDF of $h_1 \triangleq h_{sr} + \xi$, where $\xi \triangleq \alpha h_{st} h_{tr}$, is given as

$$F_{h_1}(x) = \int_0^x F_{h_{sr}}(x - z) f_\xi(z) dz. \quad (21)$$

Furthermore, invoking the CDF of h_{sr}, i.e., $F_{h_{sr}}(z) = \frac{1}{\Gamma(m_{sr})} \Upsilon(m_{sr}, \frac{m_{sr}}{\Omega_{sr}} z^2)$ and the PDF of ξ from (8) with a

simple transformation $z \to z^2$ into (21), the CDF of h_1 can be given as

$$F_{h_1}(x) = \frac{1}{\Gamma(m_{st})\Gamma(m_{tr_1})\Gamma(m_{tr_2})\Gamma(m_{sr})}$$
$$\times \int_0^x \frac{1}{z} \Upsilon\left(m_{sr}, \frac{m_{sr}}{\Omega_{sr}}(x-z)^2\right) G_{0,3}^{3,0}\left[z^2\lambda_\kappa \Big|_{m_{st},m_{tr_1},m_{tr_2}}^{-}\right] dz. \tag{22}$$

By applying the series expansion of lower incomplete Gamma function, i.e., $\Upsilon(\alpha,z) = \sum_{n=0}^{\infty} \frac{(-1)^n}{n!} \frac{z^{\alpha+n}}{\alpha+n}$ [19, eq. (8.354.1)] into (22), and solving the integral using [26, eq. (07.34.21.0084.01)], we get the CDF of h_1, as given in (9).

Moreover, the PDF of h_1 can be simply obtained by taking the derivative of (9) with respect to x using [26, eq. (07.34.20.0005.01)], as presented in (10).

ACKNOWLEDGMENT

REFERENCES

[1] I. F. Akyildiz, A. Kak, and S. Nie, "6G and beyond: The future of wireless communications systems," *IEEE Access*, vol. 8, pp. 133995-134030, 2020.

[2] A. Al-Fuqaha, M. Guizani, M. Mohammadi, M. Aledhari, and M. Ayyash, "Internet of things: A survey on enabling technologies, protocols, and applications," *IEEE Commun. Surveys Tuts.*, vol. 17, no. 4, pp. 2347-2376, 2015.

[3] M. Fallgren *et al.*, 5GCAR: Executive summary, Dec. 2019. [Online]. Available: https://5gcar.eu/wp-content/uploads/2019/12/5GCAR-ExecutiveSummary-White-Paper.pdf

[4] Y. Ye, L. Shi, X. Chu, and G. Lu, "On the outage performance of ambient backscatter communications," *IEEE Internet Things J.*, vol. 7, no. 8, pp. 7265-7278, Aug. 2020.

[5] N. Van Huynh *et al.*, "Ambient backscatter communications: A contemporary survey," *IEEE Commun. Surveys Tuts.*, vol. 20, no. 4, pp. 2889-2922, 2018.

[6] X. Wang *et al.*, "AllSpark: Enabling long-range backscatter for vehicle-to-infrastructure communication," *IEEE Internet Things J.*, vol. 9, no. 24, pp. 2552525537, Dec. 2022.

[7] X. Lu *et al.*, "Wireless-powered device-to-device communications with ambient backscattering: Performance modeling and analysis," *IEEE Trans. Wireless Commun.*, vol. 17, no. 3, pp. 1528-1544, Mar. 2018.

[8] G. Yang, Y.-C. Liang, and Q. Zhang, "Cooperative receiver for ambient backscatter communications with multiple antennas," 2017 *IEEE Int. Conf. Commun. (ICC)*, pp. 1-6, IEEE, 2017.

[9] G. Wang, F. Gao, R. Fan, and C. Tellambura, "Ambient backscatter communication systems: Detection and performance analysis," *IEEE Trans. Commun.*, vol. 64, no. 11, pp. 4836-4846, Nov. 2016.

[10] J. Qian, F. Gao, G. Wang, S. Jin, and H. Zhu, "Noncoherent detections for ambient backscatter system," *IEEE Trans. Wireless Commun.*, vol. 16, no. 3, pp. 1412-1422, Mar. 2017.

[11] W. Zhao, G. Wang, R. Fan, L.-S. Fan, and S. Atapattu, "Ambient backscatter communication systems: Capacity and outage performance analysis," *IEEE Access*, vol. 6, pp. 22695-22704, 2018.

[12] D. Li and Y.-C. Liang, "Adaptive ambient backscatter communication systems with MRC," *IEEE Trans. Veh. Technol.*, vol. 67, no. 12, pp. 12352-12357, Dec. 2018.

[13] W. U. Khan *et al.*, "Energy-efficient resource allocation for 6G backscatter-enabled NOMA IoV networks," *IEEE Trans. Intell. Transp. Syst.*, vol. 23, no. 7, pp. 9775-9785, Jul. 2022.

[14] J. Salo, H. M. El-Sallabi, and P. Vainikainen, "Statistical analysis of the multiple scattering radio channel," *IEEE Trans. Antennas Propag.*, vol. 54, no. 11, pp. 3114-3124, Nov. 2006.

[15] A. Pandey and S. Yadav, "Physical layer security in cooperative AF relay networks over mixed Nakagami-*m* and double Nakagami-*m* fading channels: Performance evaluation and optimization," *IET Commun.*, vol. 14, Issue 1, pp. 95-104, Jan. 2020.

[16] A. Pandey and S. Yadav, "Physical layer security in cooperative AF relaying networks with direct links over mixed Rayleigh and double-Rayleigh fading channels," *IEEE Trans. Veh. Technol.*, vol. 67, no. 11, pp. 10615-10630, Nov. 2018.

[17] A. Pandey, S. Yadav, D.-T. Do, and R. Kharel, "Secrecy performance of cooperative cognitive AF relaying networks with direct links over mixed Rayleigh and double-Rayleigh fading channels," *IEEE Trans. Veh. Technol.*, vol. 69, no. 12, pp. 15095-15112, Dec. 2020.

[18] T. S. Muratkar, A. Bhurane, P. K. Sharma, and A. Kothari, "Analysis of multi-tag ambient backscatter communication under time-selective fading," *IEEE Commun. Lett.*, vol. 26, no. 1, pp. 40-43, Jan. 2022.

[19] I. S. Gradshteyn and I. M. Ryzhik, *Tables of Integrals, Series, and Products*, 6th ed. New York: Academic Press, 2000.

[20] F. Fuschini, C. Piersanti, F. Paolazzi, and G. Falciasecca, "Analytical approach to the backscattering from UHF RFID transponder," *IEEE Antennas Wireless Propag. Lett.*, vol. 7, pp. 33-35, 2008.

[21] G. K. Karagiannidis, N. C. Sagias and P. T. Mathiopoulos, "N* Nakagami: A novel stochastic model for cascaded fading channels", *IEEE Trans. Commun.*, vol. 55, no. 8, pp. 1453-1458, Aug. 2007.

[22] N. Jaiswal and N. Purohit, "Performance analysis of NOMA-enabled vehicular communication systems with transmit antenna selection over double Nakagami-*m* fading", *IEEE Trans. Veh. Technol.*, vol. 70, no. 12, pp. 12725-12741, Dec. 2021.

[23] A. Pandey and S. Yadav, "Joint impact of nodes mobility and imperfect channel estimates on the secrecy performance of cognitive radio vehicular networks over Nakagami-*m* fading channels," *IEEE Open J. Veh. Technol.*, vol. 2, pp. 289-309, June 2021.

[24] M. K. Simon and M.-S. Alouini, "Digital communications over fading channels (M.K. Simon and M.S. Alouini; 2005) [Book Review]," *IEEE Trans. Inf. Theory*, vol. 54, no. 7, pp. 3369-3370, Jul. 2008.

[25] W. Rudin, *Principles of Mathematical Analysis*, 3rd edition. NewYork: McGraw-Hill, 1976.

[26] The mathematical functions site, https://functions.wolfram.com/.